

## Secondary Parameters of Type Ia Supernova Light Curves

NSF07-SNIa Collaboration

P. Höflich<sup>1</sup>, K. Krisciunas<sup>2</sup>, A. M. Khokhlov<sup>3</sup>, E. Baron<sup>4</sup>, G. Folatelli<sup>5</sup>, M. Hamuy<sup>5</sup>, M. M. Phillips<sup>6</sup>, N. Suntzeff<sup>2</sup>, L. Wang<sup>2</sup>

### ABSTRACT

High-quality observations of  $B$  and  $V$  light curves obtained at Las Campanas Observatory for local Type Ia Supernovae (SNe Ia) show clear evidence that SNe Ia with the same brightness decline or stretch may have systematic and independent deviations at times  $t \lesssim 5$  days before and at times  $t \gtrsim 30$  days after maximum light. This suggests the existence of two independent secondary parameters which control the shape of SN Ia light curves in addition to the primary light curve parameter, stretch  $s$  or  $\Delta m_{15}$ . The secondary parameters may reflect two independent physical effects caused by variations in the initial carbon-to-oxygen (C/O) profile in the progenitor and the initial central density  $\rho_c$  in a carbon-oxygen white dwarf exploding as a SN Ia. Theoretical light curves of delayed detonation SN Ia models with varying progenitor masses on the main sequence, varying accretion rates, and varying primordial metallicity reproduce two morphologically different and independent types of variations in observed visual light curves. These calculations predict small variations of  $\approx 0.05$  mag in the absolute brightness of SNe Ia which are correlated with the variations of progenitor mass on the main sequence  $M_{\text{MS}}$  which changes the C/O profile, and  $\rho_c$  which depends on the accretion rate. Such variations in real supernovae will induce systematic errors in SN Ia calibration at high redshifts. A physically motivated three-parameter,  $s$ , C/O,  $\rho_c$ , template for SNe Ia light curves might take these variations into account. Comparison between the theoretical predictions and the observational results agree qualitatively; however, the observations show variations between the  $B$  and  $V$  light curves that are

---

<sup>1</sup>Department of Physics, Florida State University, Tallahassee, FL 32306, USA pah@astro.physics.fsu.edu

<sup>2</sup>George P. and Cynthia Woods Mitchell Institute for Fundamental Physics & Astronomy, Texas A & M University, Department of Physics & Astronomy, 4242 TAMU, College Station, TX 77843, USA; krisciunas@physics.tamu.edu, suntzeff@physics.tamu.edu, lwang@physics.tamu.edu

<sup>3</sup>Department of Astronomy and Astrophysics, University of Chicago, Chicago, IL, USA; ajk@oddjob.uchicago.edu, vikram@oddjob.uchicago.edu

<sup>4</sup>Homer L. Dodge Department of Physics and Astronomy, University of Oklahoma, 440 W. Brooks, Rm 100, Norman, OK, 73019-2061 USA; baron@ou.edu

<sup>5</sup>Departamento de Astronomía, Universidad de Chile, Casilla 36D, Santiago, Chile; mhamuy@das.uchile.cl, gfolatelli@das.uchile.edu

<sup>6</sup>Las Campanas Observatory, Casilla 601, La Serena, Chile; mmp@lcoeps1.lco.cl

not expected from the modelling and may indicate limitations in the details of the theoretical models.

*Subject headings:* Supernovae: general

## 1. Introduction

SNe Ia are thought to be thermonuclear explosions of massive carbon-oxygen white dwarfs (CO-WD) in binary stellar systems. These supernovae are important tools (“standard candles”) of modern physics and cosmology. Use of SNe Ia as standard candles has provided the first direct evidence of the accelerating expansion of the universe and the existence of dark energy (Riess et al. 1998; Perlmutter et al. 1999).

Maximum luminosity varies among SNe Ia and is not a constant. Essentially all supernova-based cosmology studies use methods of calibration of SNe Ia as standardizable candles (removing luminosity variations) which rely on empirical relations between the intrinsic brightness at maximum light and other observable characteristics of SNe Ia such as the shape of the light curve, or the rate of brightness decline after maximum light – the brightness-decline relation (Phillips 1993; Phillips et al. 1999). The present accuracy of calibration,  $\sim 10\%$ , has been sufficient for discovering the Dark Energy, but it must be improved to perhaps  $\simeq 1 - 2\%$  in order to study properties of Dark Energy quantitatively. This is a formidable task which requires increasing the accuracy of SN Ia light curve observations, accounting for effects of dust absorption, and so on. It also requires improving the calibration procedure itself, which involves two important interconnected issues.

(1) If SN Ia light curves form a one-dimensional family characterized by a single parameter such as  $\Delta m_{15}$ , then the observed spread of individual SNe Ia around the average brightness-decline relation can be attributed to random statistical error, and the accuracy of cosmological measurements can be increased by simply increasing the number of observations of individual SNe Ia. On the other hand, if light curves are characterized, in addition to  $\Delta m_{15}$ , by some yet unknown independent “secondary” parameters, then improving the calibration is impossible without taking the dependence of the light curve on secondary parameters into account. So far, it is unknown if secondary parameters exist. Clear evidence for at least two independent secondary parameters will be provided in this paper.

(2) Implicit in all SN Ia calibration procedures is a fundamental assumption that nearby and distant (cosmological) SNe Ia behave identically and that empirical brightness–decline or brightness–stretch relations established for local SNe Ia can be used for high-redshift cosmological supernovae as well. Obviously, empirical studies of nearby and distant SNe Ia alone can not confirm or reject the existence of variations of brightness-decline relations with redshift. This requires independent accurate measurements of the intrinsic brightness of SNe Ia. Secondary parameters may hold a key to this difficult problem. If we understand the physical mechanisms and

the relationship of secondary parameters to initial conditions of SN Ia explosions, e.g., metallicity and/or the parameters of binary progenitors, we may gain some insights into systematic changes in SN Ia lightcurves with cosmological time.

The Carnegie Supernova Project has recently obtained a highly uniform set of SNe Ia lightcurves with an accuracy of a few hundredths of a magnitude both for individual SNe Ia and in terms of variations between different objects (Contreras et al. 2009; Folatelli et al. 2009). These new data provide clear evidence for the existence of secondary variations in SNe Ia light curves which are independent of the primary Phillips relation, and thus, are evidence for the existence of independent secondary parameters. The CSP data allow us to begin addressing issues (1) and (2) outlined above.

SN Ia models predict a weak dependence of the early light curve on the carbon-to-oxygen (C/O) ratio of the progenitor. They also predict a weak dependence of the late-time light curve on the initial central density,  $\rho_c$ , of the exploding WD. A combined analysis of new observational data and theoretical predictions leads us to suggest the existence of two independent secondary parameters that, in addition to  $\Delta m_{15}$  or stretch, control the intrinsic brightness of SNe Ia.

The paper is organized as follows: § 2 gives a short review of previous work on this subject; § 3 describes new observational data used in this paper; § 4 briefly summarizes the current theoretical understanding of SNe Ia and presents theoretical calculations of SNe Ia light curves; § 5 analyzes the observational light curves which give the evidence for the existence of secondary parameters, compares observational and theoretical light curves, and discusses the theoretical interpretation and the mechanisms by which secondary parameters arise in SNe Ia; results of the paper are summarized and the discussion of the implications of the results to the calibration of SNe Ia is presented in § 6.

## 2. Previous Work

Over the last half decade, a number of observational and theoretical studies have sought to uncover secondary parameters. Much of this effort has been in attempts to find direct correlations between physical effects and peak luminosity. Examples include metallicity (Wang et al. 1997a; Höflich et al. 1998; Timmes et al. 2003; Ellis et al. 2008; Gallagher et al. 2008; Howell et al. 2009; Piro & Bildsten 2008; Chamulak et al. 2008), asymmetries of the explosion (Wang et al. 1997b; Howell et al. 2001; Kasen et al. 2003; Kasen et al. 2004; Höflich et al. 2006; Kasen et al. 2009; Wang & Wheeler 2008), central density and C/O ratio (Höflich et al. 1998, 2000; Domínguez et al. 2001; Röpke et al. 2006; Höflich 2006), age of the progenitor (Mannucci et al. 2006; Sullivan et al. 2006), neutron-rich isotope to  $^{56}\text{Ni}$  ratio (Mazzali & Podsiadlowski 2006), and the opacity of the overlying material (Mazzali et al. 2001; Kasen & Woosley 2007). Our approach here is different. Rather than focusing on a single physical effect on a specific observable or stage, we make use of detailed stellar evolution models that were calculated all the way through white dwarf formation, accretion, and explosion (Domínguez et al. 2001; Höflich 2006) and focus on the effects that

variations in the progenitor and accretion rate have on both the early and late parts of the light curve but using parametrizations when the underlying physics is uncertain. Both approaches are valid, and we must take care not to draw conclusions beyond the range of validity of our 1-D approach and rely on consistency checks using observations. At the present time, this approach makes sense since 1-D models do a reasonable job of reproducing observations. While current 3-D models are able to reproduce some of the observations, no 3-D model to date has begun with a configuration that was the result of detailed stellar evolution, nor is it understood what physical variations in 3-D models reproduce the tight brightness-decline relation. With or without constant mixing, 1-D models can reproduce the brightness-decline relation and its narrow width (Höfllich et al. 1996; Umeda et al. 1999; Höfllich et al. 2002), a varying amount of mixing produces an ‘anti-correlation’ and/or a huge spread comparable to the entire range of SNe Ia (Höfllich et al. 1996; Pinto & Eastman 2000; Kasen et al. 2009).

Though details depend on the pre-conditioning of the WD (Höfllich & Stein 2002; Livne et al. 2005; Kasen et al. 2009; Zingale et al. 2009), 3D models of deflagrations and delayed detonations predict strong mixing of the central region during the deflagration phase (Khokhlov 2000; Gamezo et al. 2003; Reinecke et al. 2002) in conflict with observations of late time spectra (Höfllich et al. 2004; Gerardy et al. 2007) and remnants (Fesen et al. 2007). We note that recollapsing models (Bravo & García-Senz 2006; Baron et al. 2008; Bravo & García-Senz 2009; Bravo et al. 2009) avoid central mixing, but produce only  $^{56}\text{Ni}$  in the center. In these models the center has expanded sufficiently prior to carbon ignition that the electron capture rates have dropped and so burning occurs without neutronization. The gravitational confined detonation (Plewa et al. 2004; Jordan et al. 2008; Meakin et al. 2009) model will produce neutronized material under some ignition conditions and avoid its production under others (Jordan et al. 2009).

### 3. Observations

The light curves of SNe are often stitched together from observations carried out on a variety of telescopes at a variety of sites. This has the advantage of filling in gaps in the light curves. However, there is a distinct disadvantage. The spectral energy distributions of SNe are considerably different than those of normal stars, and the spectra of SNe change on time scales of days. While some spectral features are easily associated with singly and doubly ionized metals such as silicon and iron, other absorption features are actually blends of many lines. The effective bandpasses of filters vary from camera to camera. The net result is that photometry of SNe carried out on different telescopes often exhibits systematic offsets, sometimes amounting to 0.2 mag. From synthetic photometry of spectra of normal stars and spectra of SNe at different times with respect to maximum light, we can compute “S-corrections” which largely resolve these differences (Stritzinger et al. 2002; Krisciunas et al. 2003). However, unless we have good sequences of spectra for all of our SNe, it is not possible to devise error-free S-corrections. Certainly, we wish to attribute variations in light curve morphology to the SNe themselves, not to some conspiracy of the telescopes, sites, and

cameras.

The Carnegie Supernova Project (CSP), which began operation in September 2004, seeks to address this problem (Hamuy et al. 2006). The CSP endeavors to observe Type Ia and Type II-P SNe in the filters of the Sloan Digital Sky Survey (u’g’r’i’), the standard Johnson  $B$  and  $V$  filters, plus the near-infrared bands  $Y$ ,  $J$ , and  $H$ . Roughly 50 SNe are being followed each year, for five years. Almost all of the optical photometry of nearby SNe is being obtained with the Swope 1-m telescope at Las Campanas Observatory (LCO). For higher redshift SNe some  $BVI$  data are derived from images with the Wide Field CCD camera on the 2.5-m DuPont telescope at LCO, and a small amount of  $BVR$  data is from the 6.5-m Clay Telescope (Magellan #2). Based on high-quality CSP data the RMS deviations of 0.025 mag have been achieved (Contreras et al. 2009).

We use 18 SNe Ia observed in 2004, 2005, and 2006 as part of the CSP. All these had well sampled light curves. Many were observed a week or more prior to maximum light. Many were observed 60 or more days after maximum light. For the purposes of this paper we restrict ourselves to the  $B$ - and, in particular,  $V$ -band photometry because, based on theoretical models,  $V$  is expected to be least sensitive to additional variables.

The  $BVRI$  templates of SNe Ia are provided in Prieto et al. (2006). Sets of  $BVRI$  templates are characterized by the standard decline rate parameter  $\Delta m_{15}(B)$  which serves as a morphological label for the set. While Prieto et al. (2006) provide  $BVRI$  templates only  $BV$  were used in this analysis. Prior to fitting the light curves with the templates of Prieto et al. (2006) we first estimated the time of  $B$ -band maximum and subtracted the redshift- and time-dependent K-corrections from the photometry by interpolating the  $B$ - and  $V$ -band corrections of Hamuy et al. (1993). If the subsequently determined time of maximum light was more than 0.5 days different than the value adopted for the calculation of the K-corrections, then they were recalculated. It was then checked that the newly determined time of maximum light was statistically consistent and thus there was no need to iterate further.

The range of  $\Delta m_{15}(B)$  for the Prieto et al. (2006) templates is 0.83 – 1.93. For example, for a given object we chose  $B$ - and  $V$ -band templates from Prieto et al. (2006), stretched them by the time dilation factor  $(1+z)$ , then shifted them by small increments over a range of dates and over a range of magnitudes to minimize the total  $\chi^2$  of the fit in each filter. Then we tried the other templates including all bands over a range of  $\Delta m_{15}(B)$  to determine which templates give the lowest  $\chi^2$  of all. In this way we determined the observed maximum magnitudes and the times of maximum light. For each of our SNe we obtained functions that fit the  $B$ - and  $V$ -band light curves from roughly -5 until 25 days after the time of maximum light. This time interval for fitting the data was motivated by the theoretical models which predicted that, during this period, the visual LCs should be least effected by variations in the central density and the progenitors (Höflich et al. 1998; Domínguez & Höflich 2000; Höflich 2006).

For a comparison of the fits to the photometry, we then subtracted off the derived maximum magnitudes in  $B$  and  $V$ , subtracted off the times of maximum light in the two filters, and divided the

“time-since-maximum” by  $(1+z)$  to give “rest frame days since maximum”. The same normalization is applied to the photometric data.

## 4. Models of SNIa

### 4.1. Explosion

Current observations of SNe Ia favor a delayed detonation (DD) scenario of a SN Ia explosion in which the explosion begins as a subsonic deflagration which later turns into a supersonic detonation by the process of a deflagration-to-detonation transition or DDT (Khokhlov 1991). The ensuing detonation incinerates the entire WD. In one-dimensional models the deflagration speed,  $S$ , and the transition density,  $\rho_{tr}$ , at which the DDT occurs are free parameters. The value of  $\rho_{tr}$  determines the fraction of a WD that will burn to nuclear statistical equilibrium and produce  $^{56}\text{Ni}$ . Therefore,  $\rho_{tr}$  is a critical parameter that controls the brightness of a SNe Ia. DD models with  $\rho_{tr} \simeq 0.5 - 2.5 \times 10^7 \text{ g cm}^{-3}$  reproduce the observed range of SNe Ia luminosities, correct stratification of chemical elements in SNe Ia envelopes, and the correlation between maximum brightness and width of the light curve consistent with observations (Höflich 1995; Höflich et al. 1996; Mazzali et al. 1998, 2001; Höflich et al. 2002; Höflich 2006; Quimby et al. 2007; Mazzali et al. 2007; Kasen et al. 2009; Marion et al. 2009). DD models appear to be in agreement with observations of SN Ia remnants (Fesen et al. 2007; Badenes et al. 2008).

The initial central density of a WD,  $\rho_c$ , its metallicity, and its C/O ratio also influence the production of  $^{56}\text{Ni}$  and maximum brightness of SNe Ia during the explosion. Note that in our models, the free parameters are the main sequence mass of the progenitor,  $M_{\text{MS}}$ , the accretion rate, and the primordial metallicity  $Z$  (Domínguez et al. 2001; Höflich 2006). The fact that the brightness of a SN Ia is controlled, for the most part, by a single, primary parameter  $\rho_{tr}$ , and that there exists an evolutionary bottleneck associated with the limiting Chandrasekhar mass of a WD provides a plausible explanation for a near one-dimensional sequence of SN Ia explosions. A crucial point is that  $\rho_c$ , primordial metallicity, and C/O ratio influence certain characteristics of the explosion *not associated* with the primary brightness-decline relation. In particular, the C/O ratio has an influence on the expansion velocity of SNe Ia. The dependence is caused by variations in nuclear binding energy of the CO fuel. The larger the C/O ratio, the smaller the binding energy, and the faster the SN Ia envelope expands. This is a secondary effect since the bulk of the kinetic energy is determined by a much larger difference in binding energies of C/O and products of explosive burning (Fe-peak elements). On the other hand,  $\rho_c$  influences the distribution and amount of  $^{56}\text{Ni}$  in the innermost parts of a SN Ia. SN Ia models based on explosions of Chandrasekhar-mass WDs predict a hole in the  $^{56}\text{Ni}$  distribution near the center which is filled instead with highly neutronized isotopes of Fe-group elements. The hole is caused by electron captures and neutronization of matter at high densities. The size of the hole increases with  $\rho_c$ . These two effects influence the formation of both early and late portions of a light curve. As noted above the nickel hole is generally absent in

all 3-D models, either because the core expands prior to ignition, or because in delayed detonation models mixing occurs during the deflagration phase, but the stratified structure is restored by the detonation. Because the flame is very topologically complex during the deflagration phase, the detonation will not produce a central neutronized hole.

The initial C/O ratio and profile and  $\rho_c$  in a supernova are a result of stellar and binary evolution. The C/O profile is produced during the central Helium burning and thin shell burning during the stellar evolution and the accretion to  $M_{\text{Ch}}$ . The central He burning is initially dominated by carbon production via the  $3\alpha$  reaction in the convective core. When the He mass fraction becomes depleted,  $^{12}\text{C}(\alpha, \gamma)^{16}\text{O}$  mainly controls He-burning and most of the  $^{16}\text{O}$  is produced during the late phases of central He-burning. Note that the final abundances depend on a combination of the  $^{12}\text{C}(\alpha, \gamma)^{16}\text{O}$  rate and chemical mixing which determines the duration of the phase of depleted He-core burning. Stellar evolution models which produce low C/O ratios of  $\simeq 0.25 - 0.4$  are in agreement with observational constraints, like the amount of oxygen found in the inner zone of pulsating white dwarfs or the age of open clusters (Dominguez et al. 1999; Domínguez et al. 2001; Metcalfe et al. 2001; Straniero et al. 2003). The C/O ratio in the burning shell is greater,  $\approx 1$ , because the shell helium source has lower density and higher temperature compared to helium burning in the core. The size of the convective core depends mainly on the progenitor mass  $M_{\text{MS}}$  on the main sequence and, to some extent, on the primordial metallicity  $Z$ , namely the iron abundance, which dominates the opacity (Domínguez et al. 2001; Höflich et al. 2000) The dependence of  $M_{\text{core}}$  on  $M_{\text{MS}}$  is nonlinear, with the mass of the He convective core changing with  $M_{\text{MS}}$  slowly for low  $M_{\text{MS}}$  and more rapidly when  $M_{\text{MS}}$  approaches its maximum value. Approximately,  $M_{\text{core}}$  is  $0.3, 0.4, 0.7M_{\odot}$  for  $M_{\text{MS}} = 1.5, 5, 7M_{\odot}$ , respectively (Domínguez et al. 2001). The core’s C/O ratio is smallest for small  $M_{\text{MS}}$ , increases rapidly when  $M_{\text{MS}}$  increases from  $1.5$  to  $3M_{\odot}$  and remains relatively constant for larger  $M_{\text{MS}}$ . These two effects combine to make the mean C/O ratio in an exploding WD decrease with  $M_{\text{MS}}$  slowly for low mass stars  $M_{\text{MS}} \simeq 1.5 - 5M_{\odot}$  and much more rapidly for higher mass stars with  $M_{\text{MS}} \simeq 5 - 7M_{\odot}$ . In turn, this makes the explosion energy of a WD more sensitive to  $M_{\text{MS}}$  when  $M_{\text{MS}}$  is large.

The mass of the WD core is sensitive to the mass of the progenitor on the main sequence and is rather insensitive to the primordial metallicity. To first order, the C/O ratio and thus, the explosion energy decreases with  $M_{\text{MS}}$ . This tendency is generally true for  $M_{\text{MS}}$  larger than  $3M_{\odot}$  independent of assumptions about mixing and nuclear reaction rates. For lower mass progenitors, the total mean C/O ratio varies little with  $M_{\text{MS}}$ .  $M_{\text{core}}$  decreases with  $M_{\text{MS}}$ , but this effect is almost compensated by a decrease of the local C/O ratio which decreases with  $M_{\text{MS}}$ . Both this effect and the high C/O ratio in shell burning can be understood by nuclear physics and chemical mixing. The local C/O ratio depends mostly on the competition between triple- $\alpha$ ,  $3\ ^4\text{He} \rightarrow\ ^{12}\text{C}$ , and  $\alpha$ -capture on  $^{12}\text{C}$ , i.e.  $^{12}\text{C}(\alpha, \gamma)^{16}\text{O}$ . As a three-body reaction, triple- $\alpha$  dominates at high  $\alpha$  concentrations whereas  $^{12}\text{C}(\alpha, \gamma)^{16}\text{O}$  dominates when  $^4\text{He}$  is depleted (and at high temperature). During the early phases of helium core burning mostly  $^{12}\text{C}$  is produced but, eventually it is depleted by  $^{12}\text{C}(\alpha, \gamma)^{16}\text{O}$ . For burning in small convective cores, even moderate chemical mixing keeps  $^4\text{He}$  at a certain level and

prolongs the phase of  ${}^4\text{He}$  burning under depleted conditions, reducing carbon. In burning in thin radiative shells, the temperatures are higher and the burning time-scales are shorter, therefore less carbon is depleted.

The central density  $\rho_c$  at which the WD ignites is controlled by the competition between adiabatic compression caused by accumulation of mass at the surface and energy losses in the center of the WD. As a result,  $\rho_c$  depends on a configuration of the binary system, that is on the rate of accretion onto the WD from the stellar companion.

The physics of the ignition process is multi-D in nature. With the exception of Garcia-Senz & Woosley (1995) who find ignition occurs in rising plumes, all multi-D simulations to date show ignition at or near the center due to the downward motion of plumes (Höflich & Stein 2002; Zingale et al. 2009) in the simmering phase. Though relevant for the preconditioning of the explosion, variations in the final stage of runaway are of the order of hours (Höflich & Stein 2002) and unlikely to effect the central density. As a result,  $\rho_c$  depends on the configuration of the binary system, the evolutionary state of the stellar companion, and the resulting accretion rate.

In what follows, we characterize the initial conditions by  $\rho_c$ , and the progenitor characterized by the initial metallicity  $Z$  and  $M_{\text{MS}}$ . We use initial distributions of C and O in the core as predicted by the evolutionary calculations of a main sequence star with appropriate  $M_{\text{MS}}$ . Both during stellar shell burning and He burning during the accretion  $C/O \simeq 1$ . Once the stellar and WD evolution has been calculated to the onset of the explosion, the explosion is calculated using one-dimensional DD models taking into account the progenitor evolution, the hydrodynamics of the explosion, detailed nuclear networks with 213 isotopes, the radiation transport, detailed atomic models, and  $\gamma$ -ray transport. Details of the actual models are described in Domínguez et al. (2001) and Höflich (2006).

Domínguez et al. (2001) described the effects of varying the  ${}^{12}\text{C}(\alpha, \gamma){}^{16}\text{O}$  rate from the high value (Caughlan et al. 1985) used in our calculations to the lower value of Caughlan & Fowler (1988). The effect on the final compositions is large, but we use the value that has been shown to agree with observational constraints (Domínguez et al. 1999; Domínguez et al. 2001; Metcalfe et al. 2001) Note, however, that the final C/O ratio depends on both the rate and the chemical mixing scheme adopted in the stellar models (see for example Straniero et al. 2003).

## 4.2. Theoretical light curves

We calculated  $B$  and  $V$  light curves of a series of DD models with fixed  $\rho_{tr} = 2.3 \times 10^7 \text{ g cm}^{-3}$  which produce explosions with spectral and light curve characteristics of normal bright SNe Ia. Our fiducial model has  $\rho_c = 2 \times 10^9 \text{ g cm}^{-3}$ , primordial metallicity  $Z$  equal to the solar value  $Z_{\odot}$  (Anders & Grevesse 1989), and  $M_{\text{MS}} = 5M_{\odot}$ . The abundances in the WD are a result of the stellar evolution of a main sequence star with metallicity,  $Z_{\odot}$ . When scaling  $Z$ , for elements up to Si, we adopted the  $[0/\text{Fe}]$  abundance suggested by Argast et al. (2000) which implies smaller variations

with redshift for elements up to Si compared with Fe by a factor of three. This is done because  $^{22}\text{Ne}$  affects the explosive nucleosynthesis whereas Fe determines the opacity, and therefore, the size of the convective He-burning core (for a given mass) and, to some extent, the  $B$ -band magnitudes. Note that the effect of primordial metallicity  $Z$  on the explosive nucleosynthesis is dominated by the  $^{22}\text{Ne}$  abundance and not by the iron abundance because it is the reduction of the proton/nucleon ratio,  $Y_e$ , which changes the explosive equilibrium abundances. The light curves presented below illustrate the effects that variations of central density and progenitor mass,  $M_{\text{MS}}$ , have on light curves of SNe Ia.

#### 4.2.1. Influence of progenitor mass $M_{\text{MS}}$ and metallicity

Fig. 1 presents  $B$  and  $V$  light curves and  $B-V$  of four DD models with fixed  $\rho_c = 2 \times 10^9 \text{ g cm}^{-3}$  and varying  $M_{\text{MS}}$  and primordial metallicity (upper panels). The lower panels present a differential comparison of light curves normalized to maximum light. The difference is defined as  $dM(t) = M(t) - M_f(t)$ , where  $M_f$  is the magnitude of the fiducial DD model. The figure shows that variations in the progenitor, i.e. the main-sequence mass  $M_{\text{MS}}$  and metallicity, strongly change the rise to maximum light. These variations are caused by variations in expansion velocity in models with various  $M_{\text{MS}}$  and hence with various C/O ratios. The expansion velocity decreases when  $M_{\text{MS}}$  increases and the overall C/O ratio decreases. At the same time, the chemical and density structure of the outer parts of the SN Ia envelope is similar for all DD models. Therefore, variations in the formation of the early light curve are mostly controlled by the rate at which the outer layers expand and become transparent. The faster the expansion rate, the faster the photosphere recedes, and the faster the light curve rises towards maximum (see the upper left panel of Fig. 1). The light curve of the  $M_{\text{MS}} = 7M_{\odot}$  model in Fig. 1 rises notably slower than the fiducial light curve while the light curve of  $M_{\text{MS}} = 1.5M_{\odot}$  model rises somewhat faster. This is reflected as the early time negative and positive  $dM$  in the left panels of Fig. 1. The effect is more pronounced for higher  $M_{\text{MS}}$  due to the greater sensitivity of  $M_{\text{core}}$  on  $M_{\text{MS}}$  near the high end of  $M_{\text{MS}}$  interval. In particular, a strong secondary extremum develops when  $M_{\text{core}}$  extends to layers which only undergo incomplete silicon burning. As a consequence, we expect that differential effects are most pronounced in stellar populations with a mix of young and old stars, since these will contain a distribution of  $M_{\text{MS}}$ . We notice also that variations of the progenitor lead to small variations on a 10 percent level in  $B - V$  and its evolution with time (upper right panel). Changing the primordial  $Z$  will increase the primordial iron abundance in the outer layers, and, at the expense of  $^{56}\text{Ni}$ , more  $^{54}\text{Fe}$  will be produced from  $^{22}\text{Ne}$ . Primordial metallicity plays a minor role for variations in  $V$ , but  $B - V$  becomes bluer with decreasing primordial metallicity. This direct ‘photospheric’ effect does not change the visual LCs but the B and UV light curves (Höflich et al. 1998). The evolution in  $B - V$  is similar to and has been discussed in Krisciunas et al. (2003).

If we were to “observe” these four supernovae, match their light curves by applying the stretch correction, and *then* compare the residual differences we would get the result shown in the lower

right panels of Fig. 1. We show  $dM(t)$  after matching the light curves around maximum and determining the stretch over the range up to  $\simeq 15$  days past maximum light. The end result is essentially identical light curves near and past maximum with the exception of a strong deviation in the rise time for the light curve with the highest  $M_{\text{MS}} = 7M_{\odot}$  and a small deviation of the same light curve approximately 30 days past maximum. The pre-maximum deviation of the  $M_{\text{MS}} = 1.5M_{\odot}$  light curve is smaller but still visible at the level of  $\simeq 0.1$  mag.

There has long been a suspicion that the metallicity of the progenitor should be associated with the luminosity at peak (Wang et al. 2001; Hamuy et al. 1995; Branch et al. 1996). Recently attempts have been made to measure directly the average metallicity in the environment of the SN using either line indices or ratios (Hamuy et al. 2000; Gallagher et al. 2005; Gallagher et al. 2008) or by measuring the spectral energy distribution (SED) of the galaxy (Howell et al. 2009). These studies have failed to confirm the expected shift in peak luminosity with metallicity. Nuclear physics predicts that primarily due to increased amounts of the neutron rich  $^{22}\text{Ne}$  there should be a direct correlation between the amount of  $^{56}\text{Ni}$  produced and the progenitor metallicity (Timmes et al. 2003). Recent results (Howell et al. 2009; Neill et al. 2010) find a weaker than expected dependence of metallicity on  $^{56}\text{Ni}$ , whereas Gallagher et al. (2008) report a metallicity dependence in the Hubble residual, but not the peak luminosity. From the results of Argast et al. (2000) the variation of elements below Si (including Ne) varies less than Fe by about a factor of three, thus the sensitivity of the peak brightness is smaller than would be found by just scaling all elements to the iron abundance. Theoretical attempts to find correlations between metallicity and peak luminosity (or light curve shape) have not followed the detailed stellar evolution through to explosion, but have rather just altered the nucleosynthetic yields post-explosion and calculated the light curve, scaling just on the iron abundance (Kasen et al. 2009).

#### 4.2.2. Influence of central density $\rho_c$

Fig. 2 shows the same type of comparison as Fig. 1 but for a series of models with fixed  $M_{\text{MS}} = 5M_{\odot}$  and solar metallicity, and with varying accretion rate which leads to a central density  $\rho_c = 1.5 \times 10^9$ ,  $2 \times 10^9$ , and  $6 \times 10^9$  g cm $^{-3}$  which, in our models, corresponds to late-time accretion rates of  $1 \times 10^{-7} - 2 \times 10^{-6} M_{\odot} \text{ yr}^{-1}$ . Fig. 2 shows small differences between the light curves prior to maximum light. They are virtually unnoticeable in the upper panels of Fig. 2 but can be clearly seen on the differential plots (lower left panel). These differences arise due to small variations in the binding energy of WD models with different  $\rho_c$ . When  $\rho_c$  increases, so does the binding energy, and this translates into a somewhat smaller expansion velocity. As a result, light curves with larger/smaller  $\rho_c$  rise slower/faster and this results in a negative/positive pre-maximum differential  $dM$ .

We can also see that variations in  $\rho_c$  have a significant effect on the behavior of light curves which begin to show up at  $\simeq 20 - 25$  days after maximum light. Variations in  $\rho_c$  lead to a noticeable shift of the late time light curve with respect to the absolute magnitude at maximum light. The

light curves shift up or down when  $\rho_c$  decreases or increases, respectively. This effect is related to the existence of the central hole in the distribution of  $^{56}\text{Ni}$  in Chandrasekhar-mass models of SNe Ia. Due to increasing electron capture with density, the nuclear statistical equilibrium shifts away from  $^{56}\text{Ni}$  to stable isotopes of the iron group when the central density of a WD increases. Near maximum and shortly past maximum light the envelope of a SN Ia is rather opaque and  $\gamma$ -rays emitted near the center are trapped and do not contribute to the formation of the light curve. The light curve around maximum light is controlled by the distribution of  $^{56}\text{Ni}$  in the outer parts of the supernova. As time goes on, the envelope expands and the distribution of  $^{56}\text{Ni}$  near the center begins to influence the formation of the light curve. Larger central density means a larger hole and less  $^{56}\text{Ni}$ . As a result, the light curve of a SN Ia with higher  $\rho_c$  becomes shifted down with respect to maximum. With decreasing  $\rho_c$  the hole is smaller which means more  $^{56}\text{Ni}$  and the resulting shift of the light curve is positive. Note that  $B - V$  is very similar but at late times differs from the ‘general blue shift’ produced by variations in progenitors. The lower right panels of Fig. 2 again show the differentials when a stretch correction has been applied. Small pre-maximum differences in the light curves have virtually disappeared. However, shifts in the late light curves caused by variations of  $^{56}\text{Ni}$  near the center remain very pronounced.

Variations in some of the characteristics of light curves associated with variations in  $\rho_c$  and  $M_{\text{MS}}$  are summarized in Table 1. Table 1 shows that brightness of SNe Ia in both  $M_V$  and  $M_B$  increases monotonically from  $-19.25$  to  $-19.11$  and  $-19.32$  to  $-19.18$  mag, respectively, when  $M_{\text{MS}}$  decreases from  $7$  to  $1.5M_{\odot}$  when other parameters,  $\rho_{tr}$ ,  $Z$ , and  $\rho_c$ , are kept constant. These variations are of the order  $\simeq 0.1$  mag. Variations of  $M_V$  and  $M_B$  with  $\rho_c$  are smaller,  $\pm 0.03$  mag, because  $\rho_c$  mostly affects the electron-capture in the center of the SN Ia which hardly contributes to the SN Ia luminosity at maximum. The effect of metallicity  $Z$  can be seen by comparing the fiducial model (first model) of Table 1 with  $Z = 0.02$  and the fifth model with  $Z = 0.002$ .  $Z$  affects both  $M_B$  and  $M_V$  and has a pronounced influence on the  $B - V$  colors of SNe Ia.

Variations in  $\rho_c$  and  $M_{\text{MS}}$  have pronounced secondary *differential* effects on stretch-matched light curves as illustrated in Fig. 3. (1)  $M_{\text{MS}}$  influences the rise time of the light curves prior to maximum light. Larger  $M_{\text{MS}}$  leads to slower rise and vice versa. The upper right plot of Fig. 3 shows secondary variations of the absolute visual magnitude of SNe Ia,  $M_V$ , and differentials in  $M_V$  as a function of  $M_{\text{MS}}$  for times 25, 42, and 55 days past maximum light. (2) On the other hand,  $\rho_c$  influences the light curve  $\simeq 30$  days after maximum and later. Increases or decreases in  $\rho_c$  cause the later portion of the light curve to shift down or up with respect to maximum, respectively. The upper left plot of Fig. 3 shows  $M_V$ , and differentials in  $M_V$  as a function of  $\rho_c$  at 20 and 40 days past maximum light. Secondary variations in  $B - V$  for both series of models are given as a function of  $M_{\text{MS}}$  or  $\rho_c$  in the lower left plot of Fig. 3. All the plots illustrate the point that there are noticeable secondary variations of color and absolute visual magnitude of stretch-matched supernovae which are associated with variations of secondary parameters.

Finally, the lower right plot of Fig. 3 summarizes the relation of a predicted relative variation in absolute brightness of SNe Ia (the quantity which cannot be determined from observations unless

the absolute brightness of SNe Ia has been measured using an independent method of calibration) and relative secondary variations (differentials) of stretch-matched light curves of SNe Ia which may be directly accessible to observations. This plot shows that secondary variations in  $M_V$  of stretch-matched supernovae may reach 0.2 mag.

## 5. Analysis of Observations

The above theoretical considerations guide us in our differential analysis of observed light curves of SNe Ia.

Below we present a differential comparison of  $V$  and  $B$  light curves of several SNe Ia obtained by the CSP survey (Figs. 4 - 8). The basic LC properties are given in Table 2. These objects were selected because they were discovered well before maximum, have good time coverage for up to  $\simeq 60$  days past maximum light, and very small observational errors. SN 2005na serves as the reference or fiducial model for the comparison. Stretch corrections for all SNe Ia are listed in Table 1. Left panels on each figure show a comparison of light curves with stretch corrections from Table 1. Right panels show the comparison of SNe Ia after we added an additional stretch to their light curves in order to match the  $s$ -factor of the fiducial model, SN 2005na. That is, rather than just making the  $\Delta m_{15}$  stretch correction using the formulae of Jha et al. (2006), the curves were stretched such that the luminosity was brought into coincidence with SN 2005na. The additional stretch is rather small since all these objects are in the range of normal bright SNe Ia. This procedure helps reduce primary differences in due to the brightness decline relation (see § 4).

SN 2005al vs. SN 2005na (Fig. 4). These supernovae are well within the normal bright range. Early portions of their light curves, less than 25 days after maximum light, are very similar. This is also indicated by the very small difference in  $s$ -factors of these supernovae (Table 2). Exact matching gives only a marginal improvement in dispersion in  $M - M_{\text{ref}}$ . Fig. 4 shows that  $M - M_{\text{ref}}$  is less than a few hundredths of a magnitude until  $\simeq 25$  days after maximum. At later times the  $V$  light curves are shifted with respect to each other by  $\simeq 0.2$  mag. There is no discernible systematic shift in  $B$ . This behavior in  $V$  might be explained by variations in  $\rho_c$  and the size of  $^{56}\text{Ni}$  hole in the center of the SN Ia.

SN 2004ef vs. SN 2005na (Fig. 5). These two supernovae are different in their pre-maximum behavior and show an extremum between 20 and 40 days in  $V$ , both characteristics of variations in the progenitor. There might be a small systematic shift,  $\simeq 0.05$  mag, in the late portions of the  $V$  light curves as well, although it is less pronounced compared to that of the previous pair SN 2005al and SN 2005na. Differences between SN 2004ef and SN 2005na may indicate both variations in progenitor masses and metallicity, and rather similar  $\rho_c$  in these two events.

SN 2005ki vs. SN 2005na (Fig. 6). Both supernovae are very similar early on with a very small shift in the late time light curves of less than 0.1 mag. They likely have similar values of  $\rho_c$ ,  $M_{\text{MS}}$ , and metallicity.

SN 2005el vs. SN 2005na (Fig. 7) These two supernovae show differences in the early light curves, a secondary extremum, and a significant shift in the late time light curves as well. Note that the stretches of SN 2005el and SN 2004ef are very similar, making it not very likely that the huge  $M(\text{SN 2005el}) - M_{\text{ref}}$  can be attributed to differences in  $s$ . In terms of SNe Ia models, the difference hints at variations in progenitor mass  $M_{\text{MS}}$  and  $\rho_c$ .

SN 2005am vs. SN 2005el (Fig. 8). Finally, we present a differential comparison of two supernovae with a large difference in  $s$ -values. SN 2005am, is a steep decliner with  $\Delta m_{15} = 1.61$  whereas SN 2005el is a normal SNe Ia with  $\Delta m_{15} = 1.37$ . After stretching (Fig. 8), the values of  $M(\text{SN 2004am})$  and  $M_{\text{ref}}$  are surprisingly similar. Within the framework of models, this suggests similar progenitor masses and  $\rho_c$ .

Contrary to theoretical calculations which predict similar behavior of  $M - M_{\text{ref}}$  in both  $B$  and  $V$ , observations show, depending on the example, variations in the  $B$  and  $V$  morphology. At the moment the reason is not clear. Several effects may play a role: a) errors in  $s$  and the time of maximum  $t_{\text{max}}$ , b) differences in the theoretical and observational filter functions  $B$  and  $V$ , and c) limitations of the explosion models and progenitors.

First, we investigate the stability of differential comparisons of light curves. Matching the time of maximum light  $t_{\text{max}}$  of two supernovae may introduce an error in the differential comparison. Another source of the differential error may be small variations in  $\Delta m_{15}$  or  $s$ .

Fig. 9 shows the effects of a relative shift of  $t_{\text{max}}$  and a variation of  $\Delta m_{15}$  of supernovae SN 2004am and SN 2004el. These two supernovae represent a pair with different rise times and a corresponding deviation at  $\simeq 30$  days after maximum. As discussed in § 4 this may be attributed to variations in the progenitor masses of these two objects. The differentials between supernovae of various progenitors are more sensitive to uncertainties in the observables than those with the  $\rho_c$ -signature because the former show variations at both early and late times.

Maxima were shifted by  $\pm 1$  day and 2 days, and  $s$  by  $\pm 0.1$ . The figure clearly shows that the morphology of  $M - M_{\text{ref}}$  in  $V$  is stable, namely the rise, a rather flat part around maximum, and a dip at day 30. The variation of the differentials over the dip is less than 0.05 mag. For  $B$ , we still see that the main characteristics of  $M - M_{\text{ref}}$  in  $B$  are stable, namely extrema at  $\approx 15$  and 40 days, but they are larger than those in  $V$  in size, e.g., the first dip varies by almost 0.3 mag.

The difference in the shapes of  $B$  and  $V$  differentials appear to be real including the differences in  $B$  between observed and predicted morphology. In part, the size of the first  $B$ -dip may be caused by fringing, i.e. shifts of LCs with several maxima and minima, but hardly goes away.

One possible effect is a wavelength offset in the  $B$  filters. Another group of effects includes limitations inherent to the models: a) Metallicity variations for stars with the same progenitor show differences of less than 0.05 mag (Fig. 1), a value consistent with detailed spectral analyses (Lentz et al. 2001; Höflich 2006). However, uncertainties in our progenitor evolution during central He-burning may underestimate the variations in progenitors. b) In  $B$  at this level of accuracy, we

may be seeing limitations inherent in spherical models. After maximum light,  $B$  is very sensitive to temperature variations because it is formed by the Wien tail of the source function,  $S \propto e^{-h\nu/kT}$ , where  $S$  is the source function in the radiative transfer equation. For example, small variations of  $^{56}\text{Ni}$  mixing will increase the temperature and, at the same time, the blocking in  $B$ . Indeed, off-center DDT models show spectral changes in  $B$  which are compatible to the size of the deviation we find (Höflich et al. 2006; Kasen et al. 2009). However, strong rotational mixing is rather unlikely because the impact on the brightness decline relation and other observational constraints discussed in § 1. As seen above, uncertainties in the determination of  $t_{max}$  and  $s$  have moderate influence on the differential in  $V$ , but may amplify differences in  $B$ .

## 6. Discussion and Conclusions

We analyzed a set of high quality uniform  $V$  and  $B$  light curves of Type Ia supernovae obtained by the Carnegie Supernova Project. These data provide clear evidence for the existence of secondary variations in SN Ia light curves which are independent of the primary Phillips relation and, thus, for the existence of at least two independent secondary parameters. Comparison of the data with a series of non-LTE light curve calculations of delayed detonation explosions indicates that these secondary parameters may be physically related to variations of central density,  $\rho_c$  of a Chandrasekhar-mass white dwarf exploding as a SN Ia and to variations of the main sequence mass,  $M_{MS}$ , of the primary stellar companion in a progenitor binary stellar system.

It is generally accepted that the total amount of  $^{56}\text{Ni}$  produced in the explosion is the primary parameter which controls the absolute brightness and the rate of post-maximum decline. Production of nickel depends mainly on the transition density  $\rho_{tr}$  at which subsonic burning turns into a supersonic detonation. However, if  $\rho_{tr}$  were the only parameter describing the explosion we would have a perfect one-dimensional sequence of SN Ia events and a one-dimensional family of light curves. Some previous attempts to find additional parameters were done by comparing the risetimes of the nearby SNe Ia sample to that of the distant one. Riess et al. (1999) claimed to see a significant difference, however, Goldhaber et al. (2001) did not find the effect to be statistically significant.

The high quality light curves of SNe Ia obtained by the CSP clearly show that one parameter is insufficient to characterize the light curve. Light curves of several CSP supernovae shown in § 5 illustrate the fact that two supernovae with identical behavior at maximum light and the early portion of the post-maximum light curve, 0 – 30 days past maximum, may behave differently prior to maximum as well as at late times ( $> 30$  days past maximum light). In particular, SNe Ia that are similar near maximum may have different pre-maximum rise and may have the late portion of the  $V$  light curve ( $\geq 30$  past maximum light) shifted up or down by different amounts with respect to maximum. Examples presented in § 5 show that these differences may reach 0.2 – 0.3 mag.

Light curve modeling (§ 4) predicts that two supernovae with identical behavior of light curves

near maximum may exhibit small differences in the rise time to maximum and small shifts of the light curves with respect to maximum luminosity at times  $\geq 30$  days after maximum. These variations may be traced to variations in initial central density,  $\rho_c$ , and the WD progenitor mass on the main sequence,  $M_{\text{MS}}$ . Instead of  $M_{\text{MS}}$ , one may consider the carbon-oxygen ratio C/O in the pre-exploding WD as a second parameter. As far as light curves of SNe Ia are concerned, these parameters,  $\rho_c$  and  $M_{\text{MS}}$  (or C/O), may be treated as “independent” secondary parameters characterizing the light curve in addition to its main characterization via  $\Delta m_{15}$  or stretch. Theoretical predictions seem to be qualitatively consistent with two distinct morphological types of deviations shown by observations in V (§ 5). The B light curves also show distinct morphological types of deviations but the morphology appears to be different from that of the V light curves. On the contrary, light curve modeling predicts similar morphological behavior in V and B. We note that most of the energy flux is coming in the V band and thus the calculations of the V light curves should be more reliable. The reason for the discrepancy in B is not clear and requires further investigation.

The existence of independent secondary parameters in SNe Ia has several important implications. Obviously, any calibration of supernovae using a one-parameter set of light curve templates should lead to systematic errors in template matching and to calibration errors. The results of this paper indicate that a set of light-curve templates should form at least a three-parameter family. Our analysis suggests that a physically motivated set of templates may be constructed by using a primary SN Ia template parameterized by  $\Delta m_{15}$  or stretch with (1) an additional correction of the slope of the pre-maximum light curve and (2) an additional offset of the late V light curve with respect to maximum. Physically, the primary parameter  $\Delta m_{15}$  should be thought of as a parameter which reflects variations in the amount and distribution of  $^{56}\text{Ni}$  in the outer parts of the SNe Ia envelope responsible for the formation of the early post-maximum part of the light curve. The rise time correction might reflect the variation in the C/O ratio, and the offset of the light curve at later times might reflect variations in initial central density  $\rho_c$  and the amount and distribution of  $^{56}\text{Ni}$  in the central parts of the envelope.

However, producing a multi-parameter set of light-curve templates is not sufficient for improving the calibration procedure. The crucial point is that variations of initial conditions responsible for secondary parameters must also cause, according to theoretical predictions, small variations in absolute brightness of SNe Ia. The calibration must take the dependence of the absolute brightness on secondary parameters into account. By matching the proposed multi-parameter templates with high-quality observations it should be possible to account for secondary variations in the intrinsic brightness and to reduce the calibration errors. High quality data are not sufficient at this time for carrying out such a program systematically. However, this work clearly indicates the potential of high quality uniform sets of observations for studying secondary variations in SN Ia light curves and for providing important theoretical clues about physical mechanisms of such variations. One may hope that with improvements in SN Ia theory, verified with observations of nearby supernovae, it would be possible to predict variations of absolute brightness of SNe Ia as a function of secondary

parameters. This, in turn, may provide an opportunity to predict evolutionary effects in SNe Ia calibration related to systematic changes in initial conditions with redshift.

Finally, we have to address the promise and limitations of this study. Our quantitative theoretical predictions depend on our exact treatment of the explosion mechanism and stellar evolution. Thus, variations in the treatment of convection, the  $^{12}\text{C}(\alpha, \gamma)^{16}\text{O}$  rate, rotation, and 3-D explosive effects could be important at some level. Nevertheless we have tested the trends that we predict on a small number of SNe Ia and they should be tested on a large and homogeneous set of SNe Ia. Our preliminary results are promising. Light curves for a large number of SN are/will be available by projects such as the ESSENCE (ESSENCE 2009), CFH (SNLS 2009), NSNF (Aldering et al. 2002), PTF (Rau et al. 2009), and LSST (LSST 2009), and we will publish an extensive comparison. The properties of the components, i.e. the shape in  $M - M_{\text{ref}}$ , may be based on theoretical models and optimized using large data sets. However, even if our results are confirmed fully, systematic theoretical studies including 3-D effects will be essential to go further. As discussed in § 1, SN Ia physics is intrinsically 3-D and thus those effects must be taken into account. However, the last decade or so of theoretical work indicates that the effect should not be dominant since it appears from the the observations that 3-D effects like rotation of the WD and the position of initial ignition are reduced by the effects of the deflagration and DDT (Khokhlov 1995; Khokhlov et al. 1997; Niemeyer 1999; Reinecke et al. 2002; Gamezo et al. 2003; Gamezo et al. 2005; Plewa et al. 2004; Livne et al. 2005; Röpke & Hillebrandt 2005, e.g.). For a review see Höflich (2006). Finally, we return to the implications of asymmetry for the use of SNe Ia for cosmology. A 10% asymmetry of the photosphere would not cause systematic difficulties for using SNe Ia as distance indicators at the current level of accuracy of about 20% (Wang et al. 2003) though it would require that most of the dispersion has to be attributed to asymmetry. We note that if such effects are present, then SNe Ia are even more homogeneous than they seem from current dispersions in peak brightness. This level of asymmetry would, however, cause a directional dependence of the luminosity of order  $\sim 0.1$  mag (Höflich 1991) and a corresponding, but smaller, dispersion in the brightness-decline relation of SNe Ia. This dispersion depends on the viewing angle dependence of the luminosity variation and, thus, the nature of the asymmetry. The angle dependence of the luminosity due to the viewing angle  $\theta$  of a single SN Ia will not, in general, vary as the line of sight to the equator as  $\cos\theta$ . A more stringent limit comes from observations of individual supernovae. The first broad band survey by Wang et al. (1996) established that SNe Ia have very low polarization at a level of  $P \sim 0.2\%$  whereas core-collapse SNe are generally more highly polarized  $P \sim 1\%$  quality polarimetry measurements indicating that SNe Ia are more highly polarized before maximum, and a few weeks past maximum the polarization disappears (Wang et al. 2003). SN 2004dt showed that SNe Ia have spectral feature dependent polarization, implying different chemical species have different geometry (Wang et al. 2006; Patat et al. 2009). Since the continuum polarization at maximum light is observed to be  $P < 0.2\%$  which, for scattering dominated atmospheres, translates into a directional dependence of the flux at the 0.05 % level (Höflich 1991; Wang et al. 1997b, 2003; Howell et al. 2001; Wang & Wheeler 2004; Wang et al. 2006; Fesen et al. 2007; Patat et al. 2009), one expects that while 3-D effects are important for understanding the explosion mechanism, their observational

effects are relatively small. However, as summarized in Wang & Wheeler (2008) asymmetries lead to a dispersion in the color terms which can be magnified significantly when extinction corrections are applied. Other independent factors will contribute to the error and dispersion such that the interaction within the progenitor system or the primordial metallicity require early time spectra, and/or a combination of optical and IR data.

We thank the anonymous referee for a very careful reading of the manuscript and critical comments that much improved the presentation. We thank Inma Dominguez for a careful reading of the manuscript and helpful discussions and comments. The work presented in this paper has been carried out within the NSF project “Collaborative research: Three-Dimensional Simulations of Type Ia Supernovae: Constraining Models with Observations” whose goal is to test and constrain the physics of supernovae by observations and improve SNe Ia as tools for high precision cosmology. The project involves The University of Chicago (AST-0709181), the University of Oklahoma (AST-0707704), Florida State University (AST-0708855), Texas A&M (AST-0708873), The University of Chile in Santiago, and the Las Campanas Observatory, Chile. This research was also supported, in part, by the NSF grant AST-0703902 to PAH and US Department of Energy Award Number DE-FG02-07ER41517 to EB. MH and GF acknowledge support from Fondecyt (1060808 and 3090004), Programa Iniciativa Científica Milenio de MIDEPLAN’ (P06-045-F), and CONICYT (FONDAP 15010003 and PFB 06). The authors are especially grateful to the members of the Carnegie Supernova Project team for the access to observational data prior to publication.

## REFERENCES

- Aldering, G., Adam, G., Antilogus, P., et al. 2002, *Proceedings of the SPIE*, 4836, 61
- Anders, E. & Grevesse, N. 1989, *Geochim. Cosmochim. Acta*, 53, 197
- Argast, D., Samland, M., Gerhard, O. E., & Thielemann, F.-K. 2000, *A&A*, 356, 873
- Badenes, C., Hughes, J. P., Cassam-Chenaï, G., & Bravo, E. 2008, *ApJ*, 680, 1149
- Baron, E., Jeffery, D. J., Branch, D., et al. 2008, *ApJ*, 672, 1038
- Branch, D., Romanishin, W., & Baron, E. 1996, *ApJ*, 465, 73
- Bravo, E. & García-Senz, D. 2006, *ApJ*, 642, L157
- Bravo, E. & García-Senz, D. 2009, *ApJ*, 695, 1244
- Bravo, E., García-Senz, D., Cabezón, R. M., & Domínguez, I. 2009, *ApJ*, 695, 1257
- Caughlan, G. R. & Fowler, W. A. 1988, *Atomic Data and Nuclear Data Tables*, 40, 283

- Caughlan, G. R., Fowler, W. A., Harris, M. J., & Zimmerman, B. A. 1985, *Atomic Data and Nuclear Data Tables*, 32, 197
- Chamulak, D. A., Brown, E. F., Timmes, F. X., & Dupczak, K. 2008, *ApJ*, 677, 160
- Contreras, C. et al. 2009, *AJ*, in press, arXiv:astro-ph/0910.3330
- Dominguez, I., Chieffi, A., Limongi, M., & Straniero, O. 1999, *ApJ*, 524, 226
- Domínguez, I. & Höflich, P. 2000, *ApJ*, 528, 854
- Domínguez, I., Höflich, P., & Straniero, O. 2001, *ApJ*, 557, 279
- Ellis, R. S., Sullivan, M., Nugent, P. E., et al. 2008, *ApJ*, 674, 51
- ESSENCE. 2009, ESSENCE Project, <http://www.ctio.noao.edu/wproject/>
- Fesen, R. A., Höflich, P. A., Hamilton, A. J. S., et al. 2007, *ApJ*, 658, 396
- Folatelli, G. et al. 2009, *AJ*, in press, arXiv:astro-phx/0910.3317
- Gallagher, J., Garnavich, P., Berlind, P., et al. 2005, *ApJ*, 634, 210
- Gallagher, J. S., Garnavich, P. M., Caldwell, N., et al. 2008, *ApJ*, 685, 752
- Gamezo, V. N., Khokhlov, A. M., & Oran, E. S. 2005, *ApJ*, 623, 337
- Gamezo, V. N., Khokhlov, A. M., Oran, E. S., Ctchelkanova, A. Y., & Rosenberg, R. O. 2003, *Science*, 299, 77
- Garcia-Senz, D. & Woosley, S. E. 1995, *ApJ*, 454, 895
- Gerardy, C. L. et al. 2007, *ApJ*, 661, 995
- Goldhaber, G. et al. 2001, *ApJ*, 558, 359
- Hamuy, M., Folatelli, G., Morrell, N. I., et al. 2006, *PASP*, 118, 2
- Hamuy, M., Phillips, M. M., Maza, J., et al. 1995, *AJ*, 109, 1
- Hamuy, M., Phillips, M. M., Wells, L. A., & Maza, J. 1993, *PASP*, 105, 787
- Hamuy, M., Trager, S. C., Pinto, P. A., et al. 2000, *AJ*, 120, 1479
- Höflich, P. 1991, *A&A*, 246, 481
- Höflich, P. 1995, *ApJ*, 443, 89
- Höflich, P. 2006, *Nuclear Physics A*, 777, 579

- Höflich, P., Gerardy, C., Fesen, R., & Sakai, S. 2002, *ApJ*, 568, 791
- Höflich, P., Gerardy, C. L., Marion, H., & Quimby, R. 2006, *New Astronomy Review*, 50, 470
- Höflich, P., Gerardy, C. L., Nomoto, K., et al. 2004, *ApJ*, 617, 1258
- Höflich, P., Khokhlov, A., Wheeler, J. C., et al. 1996, *ApJ*, 472, L81
- Höflich, P., Nomoto, K., Umeda, H., & Wheeler, J. C. 2000, *ApJ*, 528, 590
- Höflich, P. & Stein, J. 2002, *ApJ*, 568, 779
- Höflich, P., Wheeler, J. C., & Thielemann, F. K. 1998, *ApJ*, 495, 617
- Howell, D. A., Höflich, P., Wang, L., & Wheeler, J. C. 2001, *ApJ*, 556, 302
- Howell, D. A. et al. 2009, *ApJ*, 691, 661
- Jha, S. et al. 2006, *AJ*, 131, 527
- Jordan, G. C., Meakin, C. A., Hearn, N., et al. 2009, in *Astronomical Society of the Pacific Conference Series*, Vol. 406, *Astronomical Society of the Pacific Conference Series*, ed. N. V. Pogorelov, E. Audit, P. Colella, & G. P. Zank, 92
- Jordan, IV, G. C., Fisher, R. T., Townsley, D. M., et al. 2008, *ApJ*, 681, 1448
- Kasen, D., Nugent, P., Thomas, R. C., & Wang, L. 2004, *ApJ*, 610, 876
- Kasen, D., Nugent, P., Wang, L., et al. 2003, *ApJ*, 593, 788
- Kasen, D., Röpke, F. K., & Woosley, S. E. 2009, *Nature*, 460, 869
- Kasen, D. & Woosley, S. E. 2007, *ApJ*, 656, 661
- Khokhlov, A. 1991, *A&A*, 245, 114
- Khokhlov, A. M. 1995, *ApJ*, 449, 695
- Khokhlov, A. M. 2000, *ArXiv Astrophysics e-prints*, arXiv:astro-ph/0008463
- Khokhlov, A. M., Oran, E. S., & Wheeler, J. C. 1997, *ApJ*, 478, 678
- Krisciunas, K., Suntzeff, N. B., Candia, P., et al. 2003, *AJ*, 125, 166
- Lentz, E., Baron, E., Branch, D., & Hauschildt, P. H. 2001, *ApJ*, 547, 402
- Livne, E., Asida, S. M., & Höflich, P. 2005, *ApJ*, 632, 443
- LSST. 2009, *Large Synoptic Survey Telescope*, <http://www.lsst.org/lsst>

- Mannucci, F., Della Valle, M., & Panagia, N. 2006, MNRAS, 370, 773
- Marion, G. H., Höflich, P., Gerardy, C. L., et al. 2009, AJ, 138, 727
- Mazzali, P. A., Cappellaro, E., Danziger, I. J., Turatto, M., & Benetti, S. 1998, ApJ, 499, L49
- Mazzali, P. A., Nomoto, K., Cappellaro, E., et al. 2001, ApJ, 547, 988
- Mazzali, P. A. & Podsiadlowski, P. 2006, MNRAS, L32
- Mazzali, P. A., Röpke, F. K., Benetti, S., & Hillebrandt, W. 2007, Science, 315, 825
- Meakin, C. A., Seitenzahl, I., Townsley, D., et al. 2009, ApJ, 693, 1188
- Metcalfe, T. S., Winget, D. E., & Charbonneau, P. 2001, ApJ, 557, 1021
- Neill, J. D., Sullivan, M., Howell, D. A., et al. 2010, ApJ, in press, arXiv:astro-ph/0911.0690
- Niemeyer, J. C. 1999, ApJ, 523, L57
- Patat, F., Baade, D., Höflich, P., et al. 2009, A&A, submitted, ArXiv:astro-ph/0909.5564
- Perlmutter, S. et al. 1999, ApJ, 517, 565
- Phillips, M. M. 1993, ApJ, 413, L105
- Phillips, M. M., Lira, P., Suntzeff, N. B., et al. 1999, AJ, 118, 1766
- Pinto, P. A. & Eastman, R. G. 2000, ApJ, 530, 744
- Piro, A. L. & Bildsten, L. 2008, ApJ, 673, 1009
- Plewa, T., Calder, A. C., & Lamb, D. Q. 2004, ApJ, 612, L37
- Prieto, J. L., Rest, A., & Suntzeff, N. B. 2006, ApJ, 647, 501
- Quimby, R., Höflich, P., & Wheeler, J. C. 2007, ApJ, 666, 1083
- Rau, A., Kulkarni, S. R., Law, N. M., et al. 2009, PASP, submitted, arXiv:astro-ph/0906.5355
- Reinecke, M., Hillebrandt, W., & Niemeyer, J. C. 2002, A&A, 391, 1167
- Riess, A., Filippenko, A. V., Li, W., & Schmidt, B. P. 1999, AJ, 118, 2668
- Riess, A. et al. 1998, AJ, 116, 1009
- Röpke, F. K., Gieseler, M., Reinecke, M., Travaglio, C., & Hillebrandt, W. 2006, A&A, 453, 203
- Röpke, F. K. & Hillebrandt, W. 2005, A&A, 429, L29

- SNLS. 2009, Canada-France-Hawaii Telescope Legacy Survey,  
<http://www.cfht.hawaii.edu/Science/CFHLS/>
- Straniero, O., Domínguez, I., Imbriani, G., & Piersanti, L. 2003, *ApJ*, 583, 878
- Stritzinger, M. et al. 2002, *AJ*, 124, 2100
- Sullivan, M. et al. 2006, *ApJ*, 648, 868
- Timmes, F. X., Brown, E. F., & Truran, J. W. 2003, *ApJ*, 590, L83
- Umeda, H., Nomoto, K., Kobayashi, C., Hachisu, I., & Kato, M. 1999, *ApJ*, 522, L43
- Wang, L., Baade, D., Höflich, P., et al. 2003, *ApJ*, 591, 1110
- Wang, L., Baade, D., Höflich, P., et al. 2006, *ApJ*, 653, 490
- Wang, L., Höflich, P., & Wheeler, J. C. 1997a, *ApJ*, 483, L29
- Wang, L., Howell, D. A., Höflich, P., & Wheeler, J. C. 2001, *ApJ*, 550, 1030
- Wang, L. & Wheeler, J. C. 2004, in *American Institute of Physics Conference Series*, Vol. 743, *The New Cosmology: Conference on Strings and Cosmology*, ed. R. E. Allen, D. V. Nanopoulos, & C. N. Pope, 77–87
- Wang, L. & Wheeler, J. C. 2008, *ARA&A*, 46, 433
- Wang, L., Wheeler, J. C., & Höflich, P. 1997b, *ApJ*, 476, L27
- Wang, L., Wheeler, J. C., Li, Z., & Clocchiatti, A. 1996, *ApJ*, 467, 435
- Zingale, M., Almgren, A. S., Bell, J. B., Nonaka, A., & Woosley, S. E. 2009, *ApJ*, 704, 196

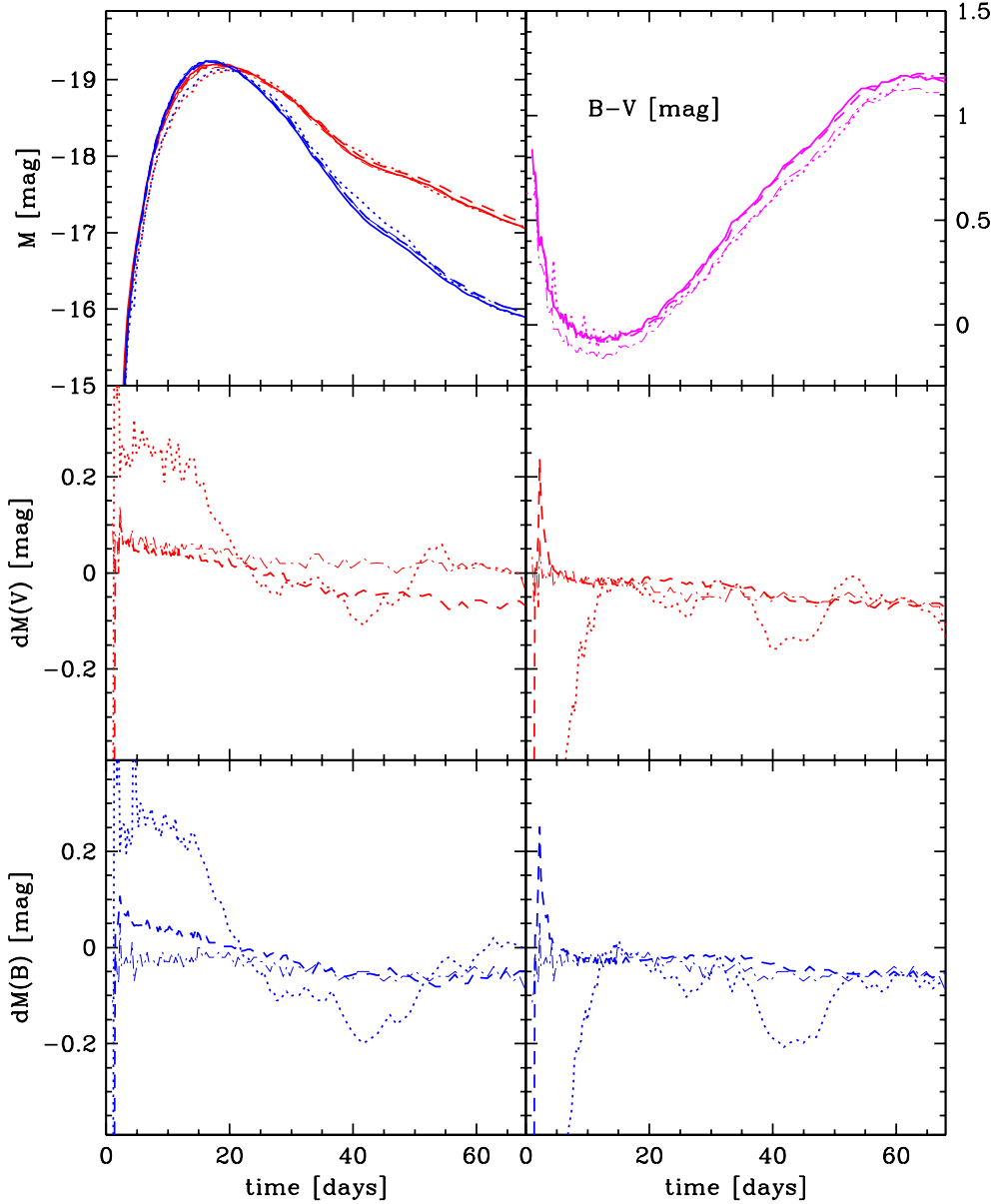


Fig. 1.—  $B$  (blue) and  $V$  (red) and  $B - V$  are given for a number of delayed detonation models with the same explosion parameters (Domínguez et al. 2001) and  $\rho_c = 2 \times 10^9 \text{ g cm}^{-3}$  (see § 4) but varying progenitor mass  $M_{\text{MS}}$  between  $1.5$  and  $7.0M_{\odot}$  and metallicities  $Z$  between  $0.002$  and  $0.02$  (solar). Models are referenced by the pair of numbers  $[M_{\text{MS}}, Z]$  for  $[1.5, 0.02]$  (dashed),  $[7.0, 0.02]$  (dotted) and  $[5.0, 0.002]$  (dash-dotted). The reference model has  $M_{\text{MS}} = 5M_{\odot}$ , and  $Z = 0.02$  (solid). The  $B$  (blue) and  $V$  (red) magnitudes and the color index  $B - V$  are given in the upper right and left panel respectively. The  $\Delta m_{15}$  for both  $V$  and  $B$  light curves are close to within  $0.03$  mag but they are not identical. The lower panels show the  $B$  and  $V$  differentials without and with stretch-correction to the  $s_f$  of the reference model on the left and right, respectively (see Table 1).

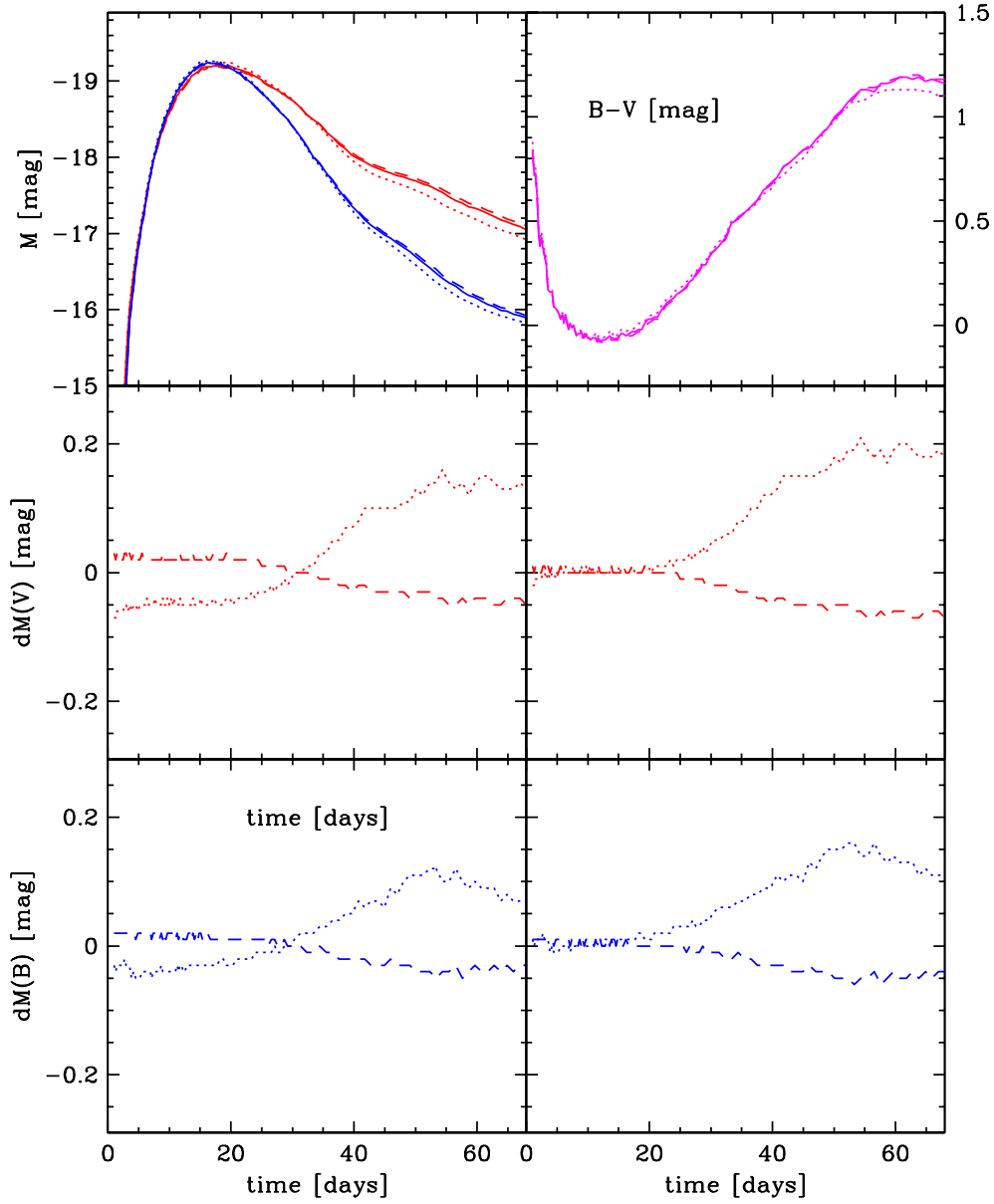


Fig. 2.— Same as in Fig. 1 but compares models with fixed  $M_{\text{MS}} = 5M_{\odot}$  and  $Z = 0.02$  and with varying central densities  $\rho_c/(10^9 \text{ g cm}^{-3})$  of 1.5 (dashed), 2.0 (solid), and 6 (dotted). The central density is due to variations in the accretion rate (see Fig. 6 of Höflich 2006).

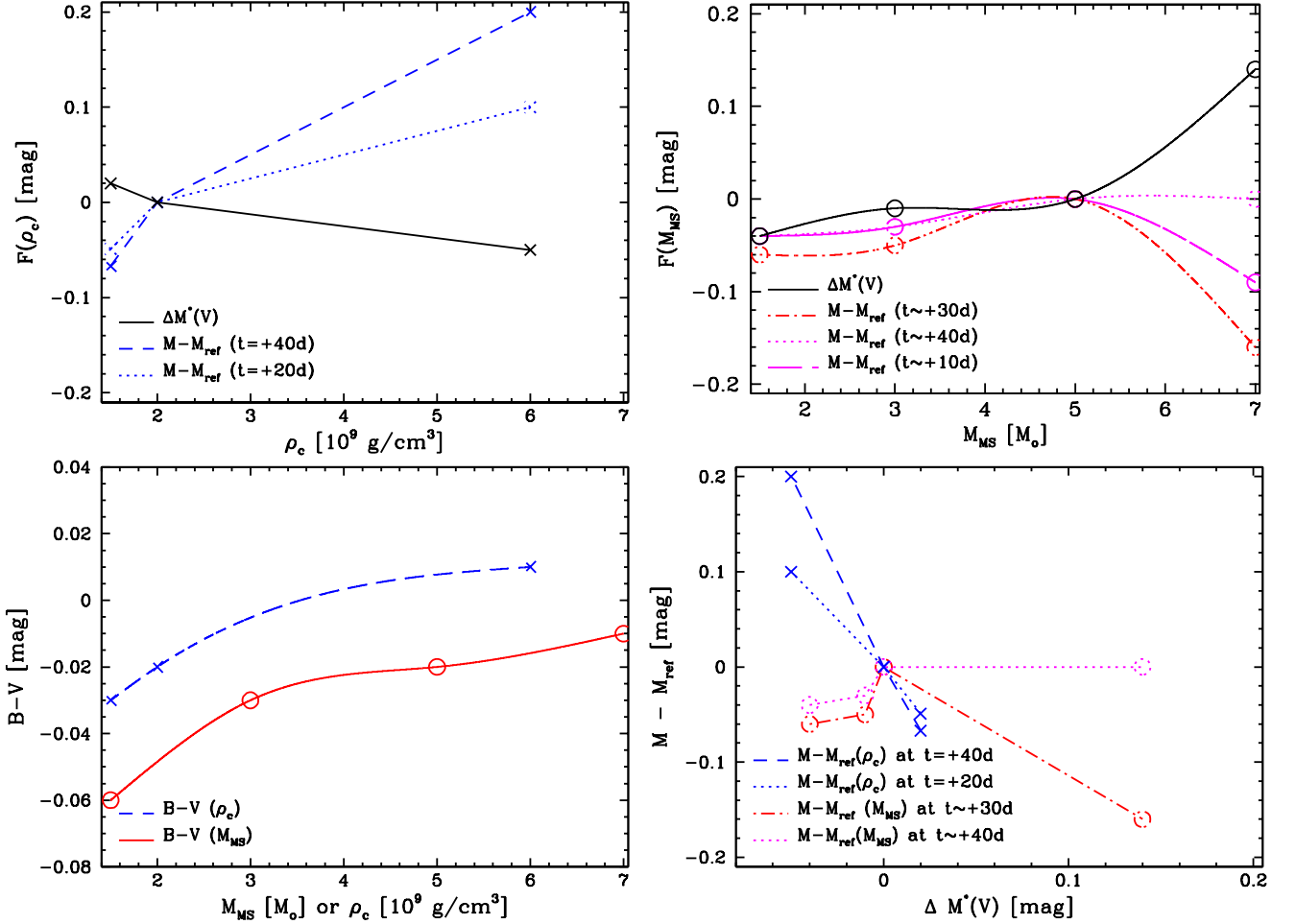


Fig. 3.— Basic observables in  $V$  for models with varying central densities  $\rho_c$  (crosses) and main sequence progenitor masses  $M_{\text{MS}}$  (open circles) relative to the reference model. All quantities are normalized to the same fiducial  $s$  factor using the brightness decline relation (Höflich et al. 2002). The change in absolute brightness at maximum light is  $\Delta M^*(V)$ , the differential brightness is  $M - M_{\text{ref}}$  at times  $+t$  after maximum light for the  $\rho_c$ -series (crosses, upper left) and the  $1^{\text{st}}$  ( $\approx +7$  days),  $2^{\text{nd}}$  ( $\approx +35$  days), and  $3^{\text{rd}}$  + 10 days for the  $M_{\text{MS}}$ -series (open circles, upper right). The corresponding colors  $B - V$  (lower left) and  $M - M_{\text{ref}}$  ( $\Delta M^*(V)$ ) (lower right) are shown. Note that the sign of the residual between two SNe Ia is arbitrary depending on the choice of a reference object.

SN2005al vs. reference SN2005na

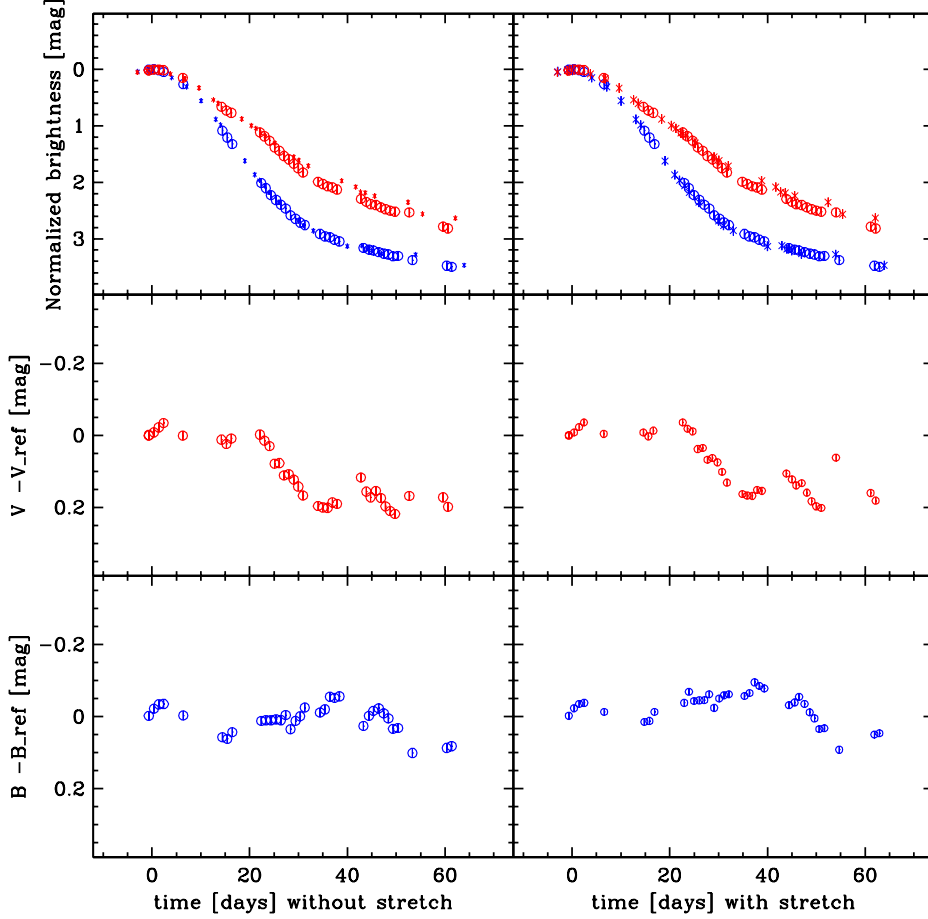


Fig. 4.— Comparison of SN 2005al to SN 2005na chosen as a reference supernova. Left column - comparison of un-normalized supernovae. Right column - comparison of supernovae normalized to the maximum brightness in V and with the  $s$ -factor of SN 2005al adjusted to be equal to the  $s$ -factors of SN 2005na. The original  $s$ -factors of all supernovae are listed in Table 2. Upper row - B and V light curves. Middle row - differential in V. Lower row - differential in B.

SN2004ef vs. reference SN2005na

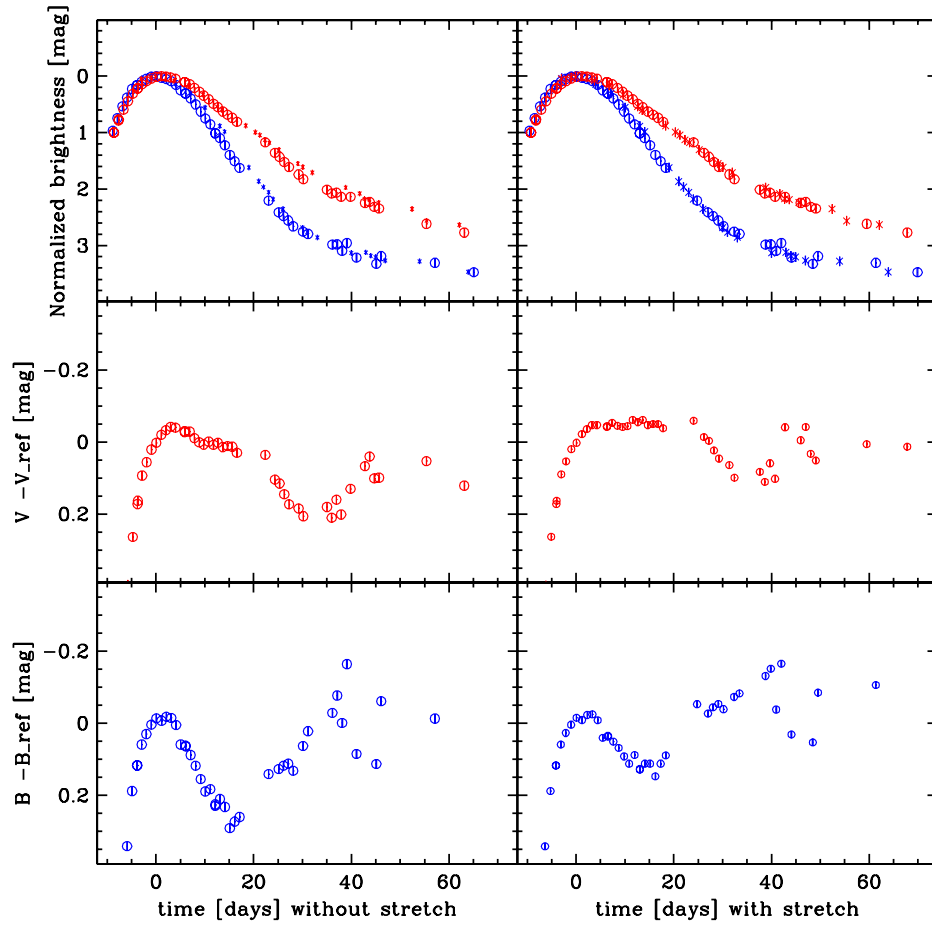


Fig. 5.— Same as Fig. 4 but comparison of SN 2004ef to SN 2005na.

SN2005ki vs. reference SN2005na

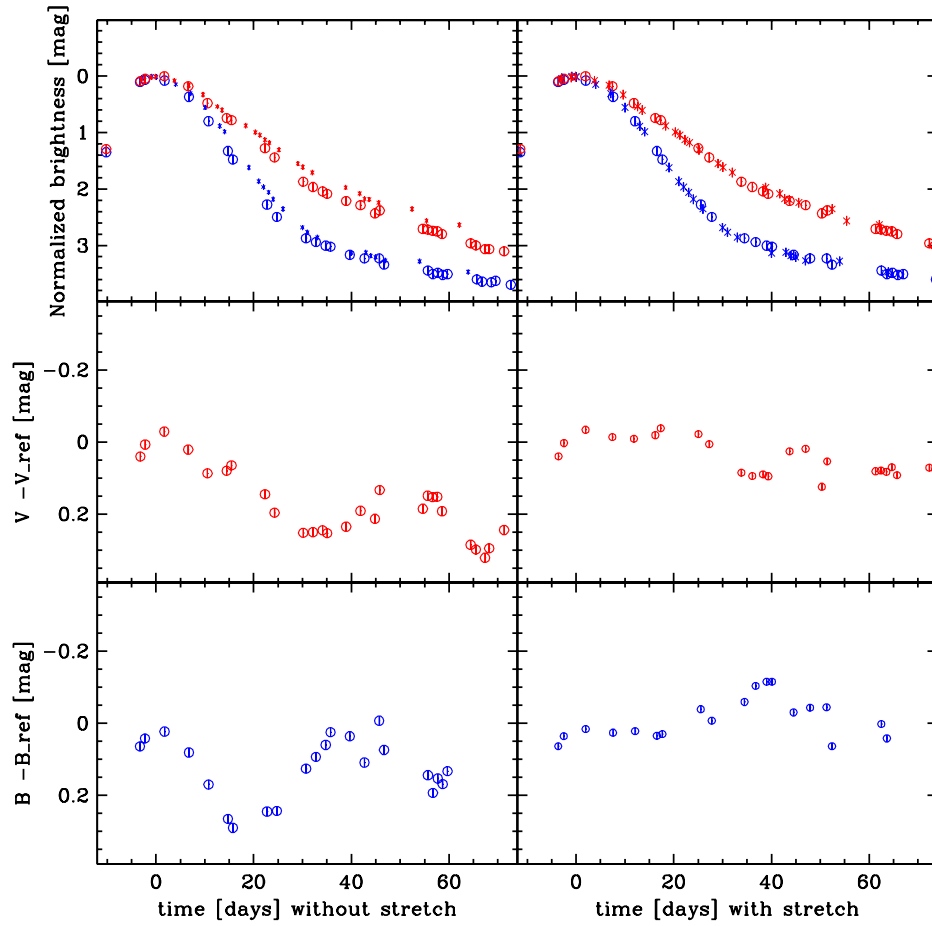


Fig. 6.— Same as Fig. 4 but comparison of SN 2005ki to SN 2005na.

SN2005el vs. reference SN2005na

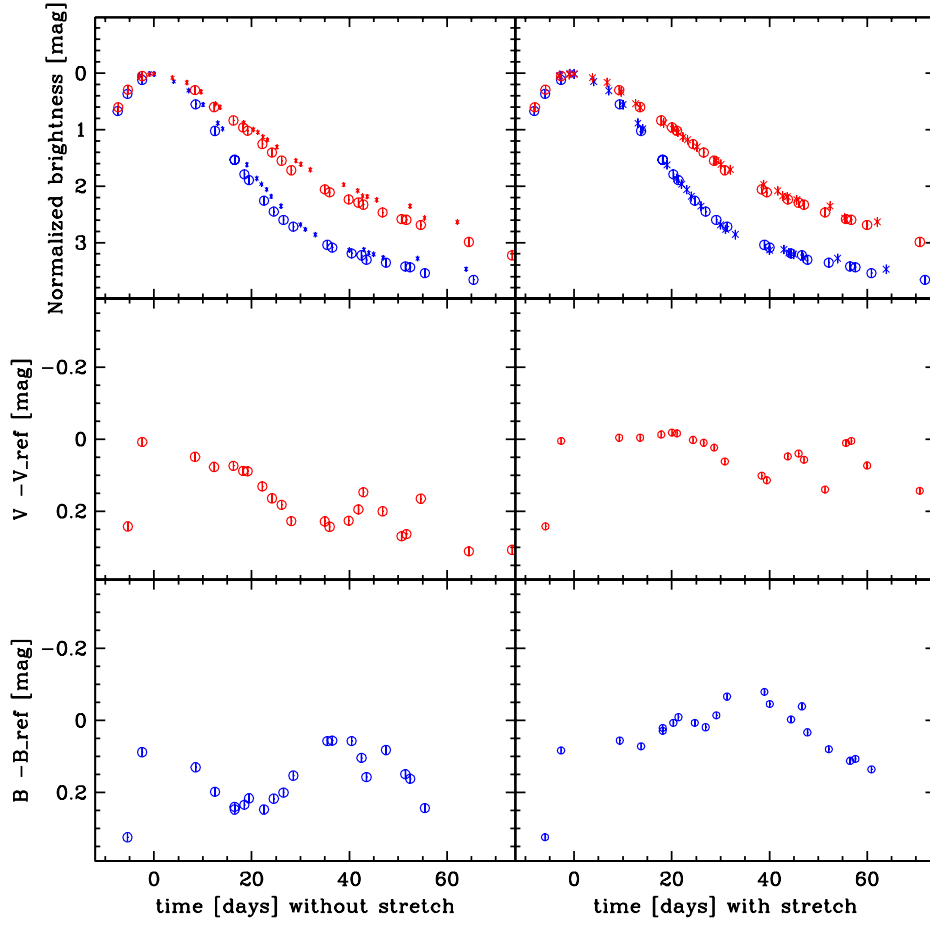


Fig. 7.— Same as Fig. 4 but for SN 2005el. Note the S-shape in  $M - M_{\text{ref}}$  with a ‘spread’ of about 0.15 mag.

SN2005am vs. reference SN2005el

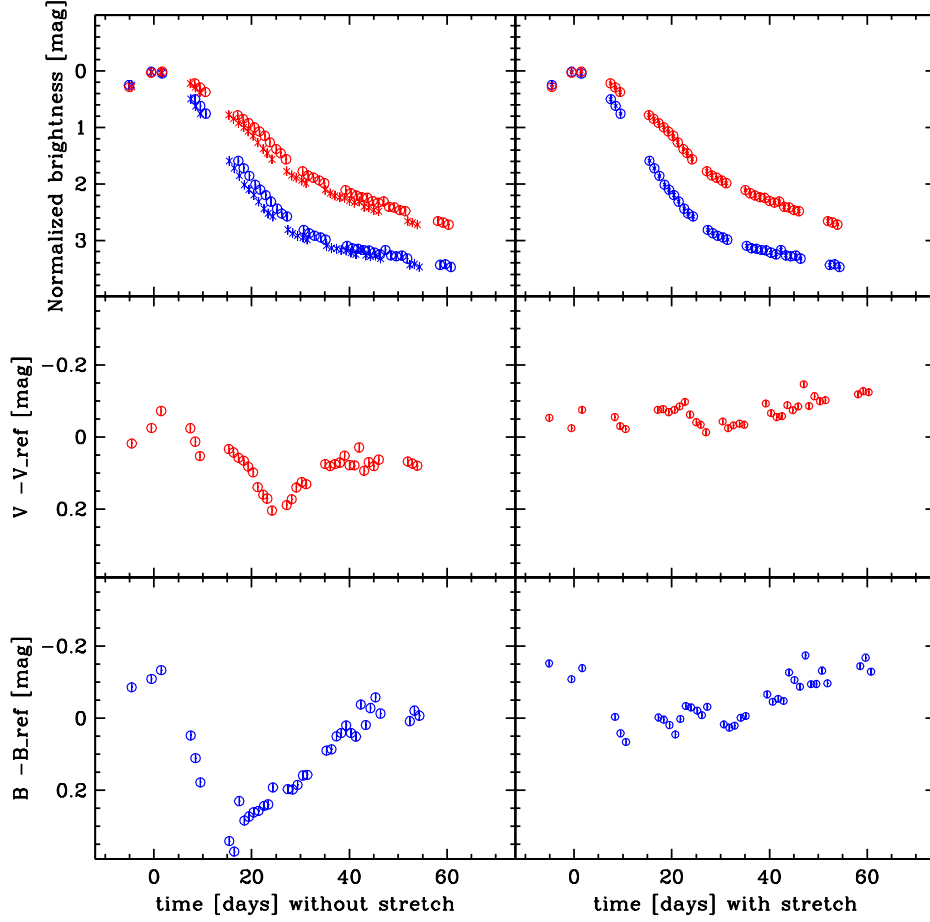


Fig. 8.— Same as Fig. 7 but comparison of SN 2005am and SN 2005el. Here, we used an offset in stretch  $s$  and in  $t_B$  of 0.01 and 0.5 days compared to Table 2, respectively. The morphology of  $M - M_{\text{ref}}$  does not change, but the graph is ‘tilted’ by about 0.1 mag.

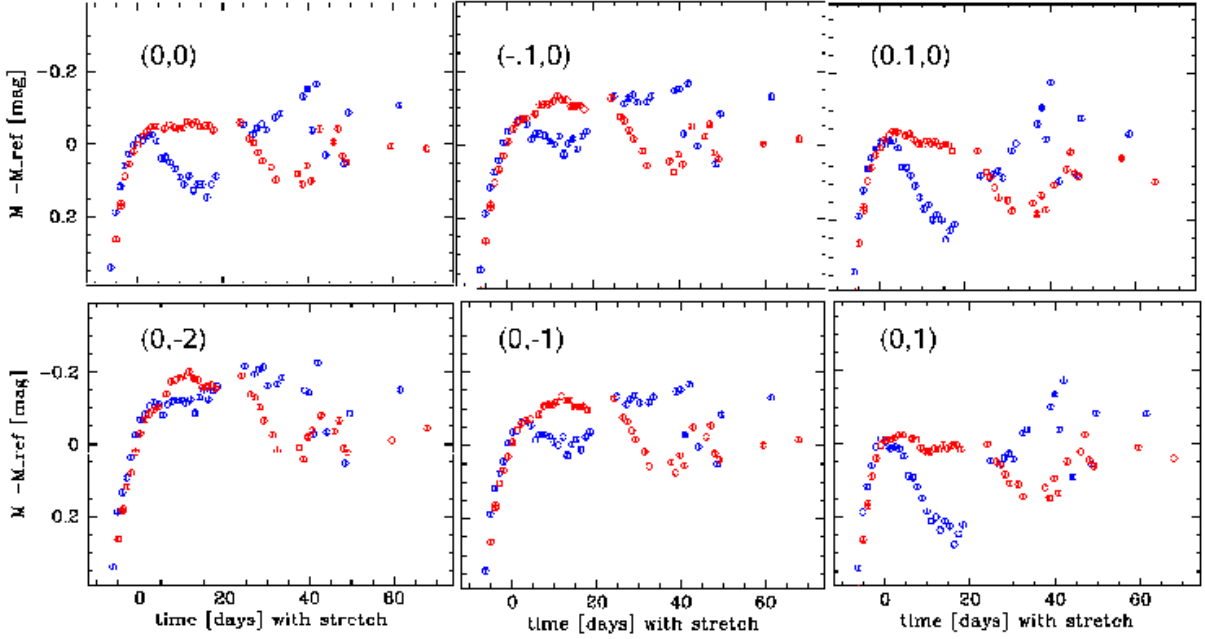


Fig. 9.— Influence of uncertainties in  $\Delta m_{15}$  and the time of maximum  $t_{max}$  on the differential comparison of SN2004ef and SN2005na (Fig. 5). Panels are marked by the assumed variations in  $\Delta m_{15}$  and  $t_{max}$ ,  $(\delta(\Delta m_{15}), \delta(t_{max}))$ . Time is in days. The functional form of the differential in  $V$  appears to be stable including the early rise, the extended plateau and the extremum at about 3 weeks past maximum. The functional form of the differential in  $B$  also appears to be stable although quantitatively the differential is more sensitive to the variations.

Table 1. Properties of Calculated SNe Ia

Parameter	Model A	Model B	Model C	Model D	Model E	Model F	Model G
$M_{\text{MS}}$	5.0	1.5	3.0	7.0	5.0	5.0	5.0
$Z$	0.02	0.02	0.02	0.02	0.002	0.02	0.02
$\rho_c$	2.0	2.0	2.0	2.0	2.0	1.5	6.0
$M_V$	-19.21	-19.25	-19.22	-19.11	-19.15	-19.19	-19.26
$t_V$	18.24	18.12	18.19	19.5	18.52	18.24	18.24
$B - V$	-0.02	-0.06	-0.03	-0.01	-0.13	0.03	0.01
$M_B$	-19.23	-19.32	-19.27	-19.18	-19.28	-19.22	-19.26
$s/s_f$	1.00	0.96	0.97	1.02	0.98	1.0	0.99

Note. — Characteristics of theoretical light curves of DD models with various progenitor mass  $M_{\text{MS}}/M_{\odot}$ , metallicity  $Z$ , and central density  $\rho_c$  in units of  $10^9 \text{ g cm}^{-3}$ . Model A is the fiducial model with  $M_{\text{MS}} = 5.0M_{\odot}$ ,  $Z = 0.02$  and  $\rho_c = 2.0 \times 10^9 \text{ g cm}^{-3}$  with  $\Delta m_{15} = 1.25$ . Listed for all models are the absolute maximum brightness  $M_{B/V}$ , time of V maximum  $t_V$  (in days), and a correction to a stretch parameter,  $s/s_f$ , required for making the  $s$ -factor of the model equal to that of the fiducial model,  $s_f$ .

Table 2. Properties of observed SNe Ia

SN	$\Delta m_{15}$ <sup>a</sup>	$s$ <sup>b</sup>	$t_B/m_B$ <sup>c</sup>	$t_V/m_V$ <sup>c</sup>	$\delta B(r/s)$ <sup>d</sup>	$\delta V(r/s)$ <sup>d</sup>
2004ef	1.47		264.96	264.54	0.09 / 0.05	0.00 / -0.03
	1.33	0.88	16.92	17.06	0.03 / -0.07	0.14 / 0.04
2005al	1.19		429.47	430.96	-0.01 / -0.02	-0.01 / -0.01
	1.24	0.92	15.08	15.08	0.01 / -0.03	0.16 / 0.13
2005am	1.56		437.10	437.53	0.12 / -0.01	0.02 / -0.07
	1.61	0.75	13.76	13.84	0.14 / -0.09	0.29 / -0.06
2005el	1.36		646.86	647.51	0.14 / 0.07	0.04 / 0.00
	1.37	0.86	15.24	15.22	0.13 / 0.02	0.24 / 0.08
2005ki	1.44		705.98	706.20	0.12 / 0.03	0.03 / -0.01
	1.41	0.85	15.69	15.65	0.10 / -0.04	0.24 / 0.07
2005na	1.19		740.32	741.79	0.00 / 0.00	0.00 / 0.00
	1.19	0.95	16.26	16.25	0.00 / 0.00	0.00 / 0.00

<sup>a</sup>Top values of  $\Delta m_{15}$  are the values for a family of  $BV$  templates for which the B-band template gives the best fit to *all* B-band data. Bottom values are derived from the “early” subset of B-data. This subset includes data which extends to the inflection point, some time 20 – 25 days after maximum light, where the second derivative of  $m_B$  changes sign.

<sup>b</sup> $s$ -factor is derived from the bottom value of  $\Delta m_{15}$  (for the early subset of B-data; see note (1)) using relation between  $s$  and  $\Delta m_{15}$  given in Jha et al. (2006).

<sup>c</sup>Time (top number) and apparent maximum brightness (bottom number) at the truncated Julian Date is “JD – 2,453,000”.

<sup>d</sup>Average difference (in mag) between  $B$  and  $V$  light curves relative to SN 2005el. Pairs of numbers are differences for raw (r) and stretched (s) data. Top pair is determined using the early subset of data. Bottom pair is determined using all data. See note (a).